Second mechanism for transitions in a reaction diffusion system

F. Marty Ytreberg and Susan R. McKay
Department of Physics and Astronomy, University of Maine, Orono, Maine 04469-5709
(Received 20 May 1998; revised manuscript received 25 August 1998)

We report two mechanisms occurring in reaction diffusion systems that lead to the same sequence of patterns, from activator rich islands to labyrinths to activator depleted well patterns. One mechanism, attributed to saturation of the activator, arises when the activator kinetics are varied and has been previously observed. The mechanism reported here occurs when the inhibitor kinetics are varied. It is signaled by an abrupt shift in the pattern roughness as each pattern emerges and little change in the characteristic wave number. The behavior of the average inhibitor and average activator concentrations also illustrates the difference between these two mechanisms. Finally, we present a quantity that shows little change when the inhibitor kinetics drive the transition, but exhibits marked changes when the activator kinetics are varied. To identify the pattern forming region, the conditions for a Turing instability are expressed simply in terms of the Jacobian and diffusion coefficient matrix for a general reaction diffusion system, and then used to confirm the results of our numerical simulations. [S1063-651X(99)02803-2]

PACS number(s): 87.10.+e, 82.20.Mj, 47.54.+r, 82.40.Ck

I. INTRODUCTION

Patterns formed by animal coats [1–3], nematic liquid crystals [4], chemical reactions [5–7], ferro fluids [8,9], and other physical systems are qualitatively very similar. A common feature in these systems is the presence of two or more competing elements. These elements can be described generically as the activator and the inhibitor [1], with the activator possessing self-enhancing or autocatalytic behavior and the inhibitor diffusing rapidly compared to the activator and squelching its spread.

Mathematically, this type of behavior is captured by a two-component reaction diffusion system

$$a_t = D_a \nabla^2 a + f(a,h), \tag{1a}$$

$$h_t = D_h \nabla^2 h + g(a,h), \tag{1b}$$

in which f and g are the kinetics linking the activator a and the inhibitor h, which will always be nonlinear [2]. Patterns can form in this system due to a Turing instability, in which the system is stable to small perturbations from the steady state in the absence of diffusion but unstable when diffusion is present [10,2]. The premise is that perturbations from the steady state grow exponentially until the nonlinear terms become significant growth limiters, leading to spatial inhomogeneities in concentrations [2]. This and other scenarios for pattern formation have been confirmed by simulations of systems of this form, such as the Gierer-Meinhardt (GM) model [1], the Gray-Scott model [11], and the Fitzhugh-Nagumo model [12,13]. Patterns can be formed by wave front interactions of two competing steady states [12] or by local activator and/or inhibitor concentrations [1,11,13].

In the current study, we present patterns seen by simulation of the GM model, and then show how, within the Turing region, the transitions in the island to labyrinth to well sequence can occur in two different ways depending upon whether the transition is driven by the activator or the inhibitor kinetics. Included in the Appendix are the conditions required for a Turing instability in a general reaction diffusion system written simply in terms of the Jacobian and diffusion matrices.

II. COMPARISONS OF TRANSITIONS DRIVEN BY KINETICS

Linear stability analysis (Appendix, [2]) and simulations can be used to identify the parameter regions in which Turing patterns can occur. As an example, the GM model in dimensionless form [1,14], with basic production terms set to zero can be written as

$$a_t = D\nabla^2 a + \frac{a^2}{(1+\kappa a^2)h} - a, \tag{2a}$$

$$h_t = \nabla^2 h + \mu(a^2 - h). \tag{2b}$$

The parameter κ allows the activator to saturate, D is a ratio of the diffusion coefficients of the activator and inhibitor (D_a/D_h), and μ is a ratio of the removal rates (μ_h/μ_a). Figure 1 illustrates the agreement between the region of the Turing instability, as obtained by linear stability analysis (solid lines), and the boundary of the pattern formation region determined from our simulations (squares). The hatched region indicates where all of the conditions for a Turing instability are met.

Previous studies [1] have indicated that islands of higher activator concentration form for $\kappa = 0$, and labyrinth patterns occur due to saturation effects once κ is sufficiently increased from zero. Previously unreported though is the existence of labyrinth patterns occurring at $\kappa = 0$, which we have obtained by changing the ratio of removal rates μ in the inhibitor kinetics. Figure 2 illustrates the regions of parameter space in which various patterns form. In region I, stable activator rich islands form for small κ [Fig. 3(a)]. As κ increases, local activator levels saturate, islands merge, and activator rich regions are more likely to have activator rich neighbors. Patterns within region II evolve from the merging

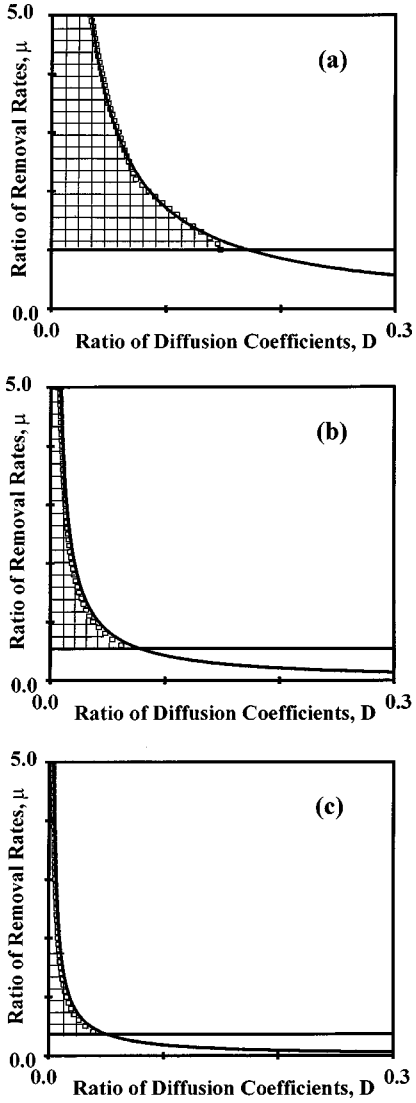

FIG. 1. Comparison of the region of the Turing instability, as obtained by linear stability analysis (solid lines), and the boundary of the pattern formation region determined from our simulations (squares) for the Gierer-Meinhardt model. The hatched region indicates where all of the conditions for a Turing instability are met. (a) $\kappa=0.0$, (b) $\kappa=0.5$, and (c) $\kappa=1.0$.

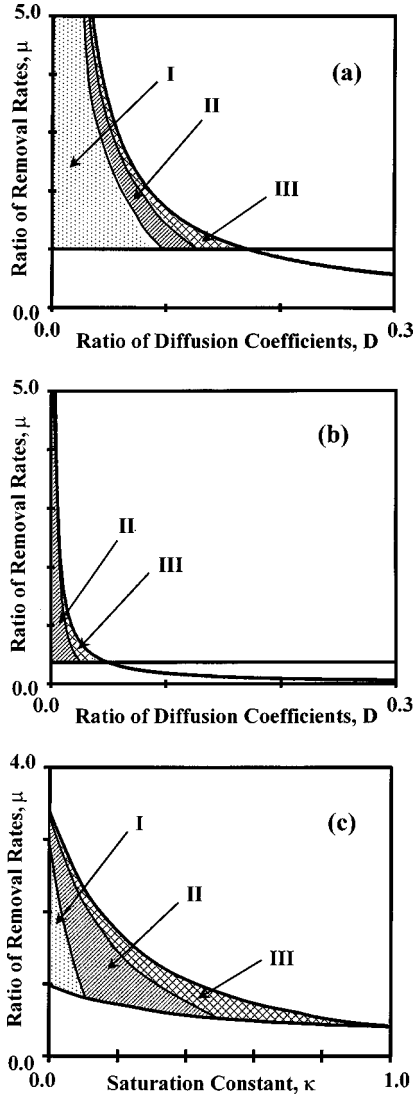

FIG. 2. Results of computer simulation of the Gierer-Meinhardt model given by Eq. (2). Patterns include spots or islands (region I), labyrinth or coexisting islands and labyrinths (region II), and well patterns (region III). (a) Phase diagram in μ-D space for $\kappa=0.0$. (b) Phase diagram in μ-D space for $\kappa=1.0$. (c) Phase diagram in μ-κ space for $D=0.05$.

of the islands of Fig. 3(a) and are characterized by elongated structures or stripes [Fig. 3(b)]. In this region, there are several other varieties of patterns that may form, depending upon parameter values and the initial conditions. For small values of μ, the most prevalent pattern contains stripes, which may be straight [Fig. 3(c)] or wavy [Fig. 3(d)] depending upon initial conditions. For larger μ, fully connected labyrinth patterns [Fig. 3(e)] dominate, however, spiral-like patterns [Fig. 3(f)] and stripes are also observed. For $\kappa=1.0$, labyrinth segments and full labyrinth structures are also seen [Figs. 3(h,i)]. These patterns, although qualitatively similar to those for $\kappa=0.0$, contain more defects. We have tested a range of system sizes, from 40×40 to 500×500, and find that labyrinths are favored over stripes in larger systems. Region III is populated by a well pattern, formed by activator depleted regions [Fig. 3(g)]. All of these patterns are stationary.

The simulations are done using a finite difference approximation of Eq. (2) with periodic boundary conditions (see [15]). Patterns shown are developed from initial conditions given by random spatial fluctuations ($\pm10\%$) about the steady state for a and h, and simulations are run for 100 000 time steps allowing all of the patterns to form fully. Other random initial conditions give qualitatively the same patterns for the same parameter choices.

Within the region of Turing patterns, of particular interest are the mechanisms that lead to transitions from one type of pattern to another. Using the GM model as an example, we show that changes in kinetics lead to two qualitatively different types of transitions from island to labyrinth to well patterns. The first occurs as κ is increased while D and μ are fixed and can be understood in terms of allowing the activator to saturate at lower values. This mechanism has been discussed previously (see [1]). The second is seen by increasing μ with κ and D fixed and corresponds to an increase in the rate at which the inhibitor is removed from the system. A

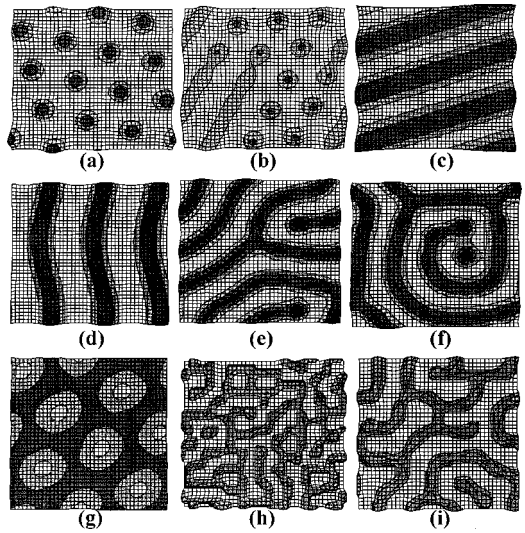

FIG. 3. Examples of patterns on a 40×40 grid with gray scale indicating concentration of the activator; higher-density regions are darker. (a) Island pattern; $\kappa=0.0$, $\mu=2.0$, and $D=0.05$. (b) Merging islands; $\kappa=0.0$, $\mu=4.0$, and $D=0.036$. (c) Stripe pattern; $\kappa=0.0$, $\mu=2.0$, and $D=0.08$. (d) Wavy stripes; $\kappa=0.32$, $\mu=1.1$, and $D=0.04$. (e) Labyrinth pattern; $\kappa=0.0$, $\mu=5.0$, and $D=0.031$. (f) Spiral-like labyrinth; $\kappa=0.0$, $\mu=5.0$, and $D=0.032$. (g) Well pattern; $\kappa=0.0$, $\mu=2.0$, and $D=0.085$. (h) Labyrinth segments; $\kappa=1.0$, $\mu=2.0$, and $D=0.004$. (i) Defect-rich labyrinth; $\kappa=1.0$, $\mu=1.0$, and $D=0.007$.

look at Eq. (2b) shows that μ can be thought of as the strength of the inhibitor kinetics. An increase in μ both increases the amount of inhibitor produced in activator rich regions, and decreases the amount of inhibitor produced in inhibitor rich regions. These features can combine to produce an effect similar to enhanced saturation of the activator.

Both of these transitions can be understood by examining Fig. 2(c). Although the sequences of patterns are the same in these two cases, there are quantities in which distinct differences can be seen depending upon whether the activator kinetics κ or inhibitor kinetics μ are driving the transitions. The following sections describe these quantities and how they differ for the choice of driving parameter.

A. Characteristic wave number

The range of wave number that grows, obtained using linear stability analysis as shown in the Appendix, can be plotted as a function of our two driving parameters κ and μ. Figure 4 shows this range as well as the fastest growing wave number (i.e., largest ω). For both of these plots, the transitions from island to labyrinth to well patterns take place moving from left to right on the graphs.

When the transitions are driven by κ we see that the fastest growing wave number increases [Fig. 4(a)]. This trend is verified in simulations where the island size changes as a function of κ. On the other hand, the fastest growing wave number remains essentially constant as a function of μ [Fig. 4(b)] and, once again, simulations verify this feature by exhibiting constant island size. These results suggest that increases in κ change the island size until a critical size is obtained above which the islands must begin to merge, whereas increases in μ prevent islands from growing by providing more inhibitor in activator rich regions.

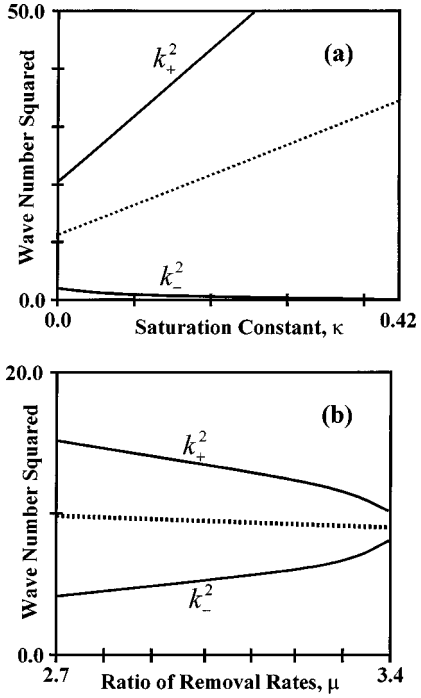

FIG. 4. Range of wave number that can grow according to linear stability analysis for qualitatively similar series of transitions between patterns. Solid lines define this range with k_+ and k_- representing, respectively, the largest and smallest wave number allowed to grow, while the dotted line shows the fastest growing wave number as a function of driving parameter with fixed $D=0.05$. (a) Driving parameter is κ with $\mu=1.0$. (b) Driving parameter is μ with $\kappa=0.0$.

Another distinct difference is that driving the transitions with κ moves the system away from the Turing point ($k_+=k_-$), increasing the range of wave number that can grow. However, when driving the transitions with μ, the system moves toward the Turing point, decreasing the range of wave number that can grow.

B. Average concentration

Pattern sequences driven by either κ or μ are accompanied by discontinuities in the slope of the average activator and inhibitor concentrations at each transition (Fig. 5). The pattern change corresponding to a slope discontinuity can be as subtle as the rearrangement of islands or as dramatic as labyrinths breaking up to form wells.

Using κ as the driving parameter [Fig. 5(a)], we see the average inhibitor concentration fall off very rapidly as κ is increased from zero. If μ is driving the transition [Fig. 5(b)], we see a different trend in which the average activator and inhibitor concentrations mirror each other in the sense that the changes taking place in the average activator concentration also take place in the average inhibitor concentration.

C. Pattern roughness

Another important difference is seen in the pattern roughness, defined as $R=\int(|\vec{\nabla}a|^2+|\vec{\nabla}h|^2)d\vec{r}$ (see [16] and [2]). This is not an energy in the Liapunov or Hamiltonian sense

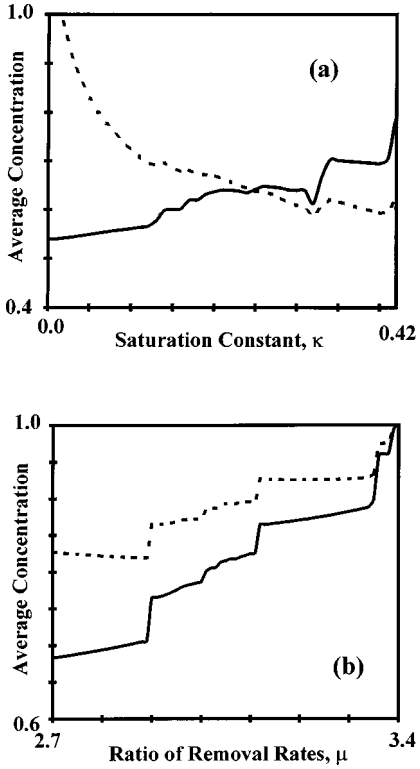

FIG. 5. Average activator (solid line) and inhibitor (dotted line) concentrations as a function of driving parameter with fixed $D=0.05$. (a) Driving parameter is κ with $\mu=1.0$. (b) Driving parameter is μ with $\kappa=0.0$.

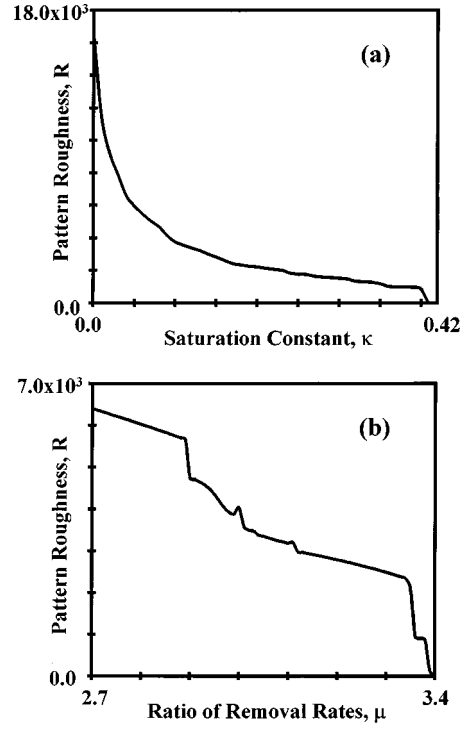

FIG. 6. Pattern roughness, defined in the text, as a function of driving parameter for transitions between patterns with fixed $D=0.05$. (a) Driving parameter is κ with $\mu=1.0$. (b) Driving parameter is μ with $\kappa=0.0$.

but rather a quantitative measure of the inhomogeneity of the pattern. As shown in Fig. 6, this roughness remains smooth through the transitions as κ is varied, but can display sharp jumps if changes in μ are driving the transitions. The magnitudes of these jumps are sensitive to the details of the initial conditions. This difference can be understood in light of what was said earlier about the island size changing as a function of κ but not μ.

D. Variational approach

Using a variational approach, any reaction diffusion system in the form of Eq. (1) can be written as

$$a_t=-\frac{\delta E_a}{\delta a},\quad h_t=-\frac{\delta E_h}{\delta h}. \tag{3}$$

For the GM model, E_a and E_h become

$$E_a=\int\left[\frac{1}{2}D_a|\vec{\nabla}a|^2-\frac{1}{h\sqrt{\kappa}^3}[a\sqrt{\kappa}-\arctan(a\sqrt{\kappa})]+\frac{1}{2}a^2\right]d\vec{r}, \tag{4a}$$

$$E_h=\int[\tfrac{1}{2}D_h|\vec{\nabla}h|^2-\mu(a^2h-\tfrac{1}{2}h^2)]d\vec{r}. \tag{4b}$$

In the case of stationary patterns ($a_t=0$ and $h_t=0$), [16] can be applied and Eq. (4) reduces to

$$E_a=\int\left[\frac{a^3}{2h}\frac{1}{1+\kappa a^2}-\frac{1}{h\sqrt{\kappa}^3}[a\sqrt{\kappa}-\arctan(a\sqrt{\kappa})]\right]d\vec{r}, \tag{5a}$$

$$E_h=\int[-\mu a^2h]d\vec{r}. \tag{5b}$$

A graph of $\sqrt{E_a^2+E_h^2}$ for stationary patterns [from Eq. (5)], shown in Fig. 7, displays dramatic change (power law decay) of this quantity when the transitions are driven with κ. This same quantity shows little change (varying by only 15% through entire scan range of μ), however, when the transitions are driven with μ. It is worth mentioning that a gradient system with a Liapunov functional ($E_a=E_h$) requires that $\partial f/\partial h=\partial g/\partial a$. However, for a to be the activator of h, $\partial g/\partial a>0$, and for h to be the inhibitor of a, $\partial f/\partial h<0$. Thus no activator-inhibitor system [including Eq. (2)] can be written as a gradient system with a Liapunov functional.

III. CONCLUSIONS

We have shown that a classic activator-inhibitor system can produce a wide variety of Turing patterns, with transitions occurring by two different mechanisms, activator saturation or inhibitor removal. Distinct differences between these mechanisms are quantified using the GM model as an example. Transitions driven by activator saturation are characterized by smooth changes in the apparent wavelength of

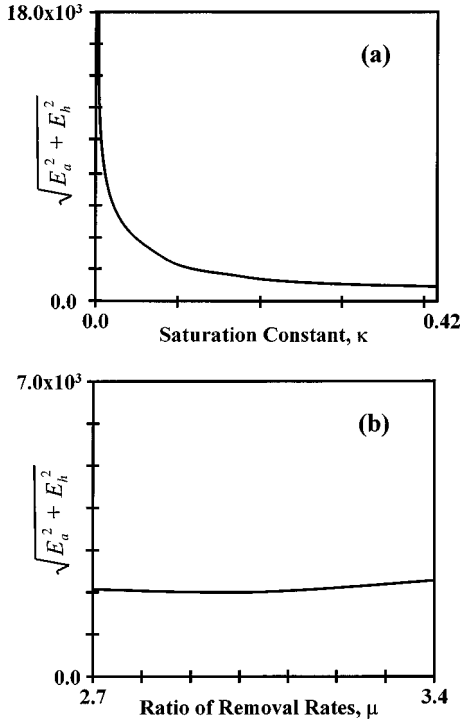

FIG. 7. Quantity $\sqrt{E_a^2+E_h^2}$ as a function of driving parameter for transitions between patterns with fixed $D=0.05$. (a) Driving parameter is κ with $\mu=1.0$. (b) Driving parameter is μ with $\kappa=0.0$.

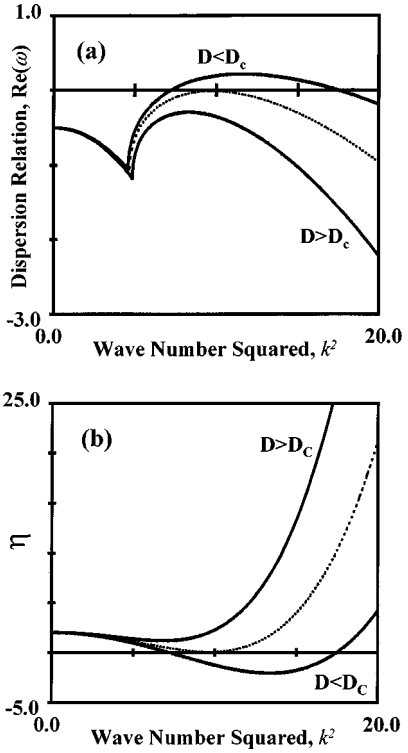

FIG. 8. (a) Dispersion relation obtained using linear stability analysis from the Gierer-Meinhardt model shown for values of D greater than, less than, and equal to (dashed line) the critical D, D_c. Regions of positive ω indicate cases in which fluctuations will grow possibly forming an inhomogeneous pattern. (b) $\eta(k^2)$, function used to determine quantities such as k_0 associated with the fastest growing mode.

the pattern, while transitions due to increasing the inhibitor removal rate exhibit no change in the apparent wavelength of the pattern.

Our simulations are in excellent agreement with the general conditions for a Turing instability, derived for a two-component reaction diffusion system using linear stability analysis.

APPENDIX

Linear stability analysis for Eq. (1) yields the dispersion relation

$$2\omega(k^2)=\tau_A-k^2\tau_D\pm\sqrt{(\tau_A-k^2\tau_D)^2-4\eta(k^2)}, \tag{A1a}$$

$$\eta(k^2)=\Delta_A-k^2(\tau_A\tau_D-\tau_{AD})+\Delta_D k^4, \tag{A1b}$$

where τ is used to represent the trace of the matrix noted in the subscript and likewise Δ represents the determinant. The matrix D is a diagonal matrix of the diffusion coefficients and A is the Jacobian matrix of f and g.

For a Turing instability (compare to [1,2]), in the absence of diffusion ($k^2=0$), the requirement that $\omega<0$ leads to two conditions, $\tau_A<0$ and $\Delta_A>0$. If diffusion is present ($k^2>0$), then $\omega>0$ for a Turing instability. With the restrictions imposed by the first two conditions, the third can occur only if $\eta<0$ for some range of wave number. A typical graph of $\eta(k^2)$ and the real part of $\omega(k^2)$, done for the GM model [Eq. (2)], is shown in Fig. 8 and illustrates that for Turing patterns it is sufficient to require that the minimum value of $\eta<0$. The wave number k_0 associated with the minimum value of η, η_0 is given by $k_0^2=(\tau_A\tau_D-\tau_{AD})/2\Delta_D$.

Since k must be real, the condition $\tau_A\tau_D-\tau_{AD}>0$ must be met. Substituting k_0^2 into Eq. (A1b) yields $\eta_0=\Delta_A-(\tau_A\tau_D-\tau_{AD})^2/4\Delta_D<0$ which provides our last condition (actually two conditions due to the quadratic), $(\tau_A\tau_D-\tau_{AD})^2-4\Delta_D\Delta_A>0$.

When these four conditions are satisfied, a range of wave number $k_-^2<k^2<k_+^2$ exists for which perturbations from the steady state will grow exponentially with the possibility of patterns forming due to the nonlinear kinetics. This range can be determined from the zeroes of η as

$$k_\pm^2=\frac{1}{2\Delta_D}(\tau_A\tau_D-\tau_{AD}\pm\sqrt{(\tau_A\tau_D-\tau_{AD})^2-4\Delta_A\Delta_D}). \tag{A2}$$

For a finite system discrete values of k are allowed, which depend on the boundary conditions and system size. If the system does form a Turing pattern, it will be characterized by a wave number within the range given by Eq. (A2).

[1] A. J. Koch and H. Meinhardt, Rev. Mod. Phys. **66**, 1481 (1994).
[2] J. D. Murray, *Mathematical Biology* (Springer-Verlag, New York, 1989).
[3] J. D. Murray, *Lectures on Nonlinear-Differential-Equation Models in Biology* (Clarendon Press, Oxford, 1977).
[4] L. Carlotti, S. Faetti, and M. Nobili, J. Phys. II **6**, 235 (1996).
[5] K. J. Lee and H. L. Swinney, Phys. Rev. E **51**, 1899 (1995).
[6] R. Kapral, Physica D **86**, 149 (1995).
[7] A. Belmonte, J.-M. Flesselles, and Q. Ouyang, Europhys. Lett. **35**, 665 (1996).
[8] R. E. Rosenswieg, *Ferrohydrodynamics* (Cambridge University Press, New York, 1985).
[9] D. P. Jackson, R. E. Goldstein, and A. O. Cebers, Phys. Rev. E **50**, 298 (1994).
[10] A. M. Turing, Philos. Trans. R. Soc. London, Ser. B **237**, 37 (1952).
[11] J. E. Pearson, Science **261**, 189 (1993).
[12] C. Elphick, A. Hagberg, and E. Meron, Phys. Rev. E **51**, 3052 (1995).
[13] R. E. Goldstein, D. J. Muraki, and D. M. Petrich, Phys. Rev. E **53**, 3933 (1996).
[14] A. Gierer and H. Meinhardt, Kybernetik **12**, 30 (1972).
[15] Step sizes used were $\Delta t = 0.01$ and $\Delta x = 1/\sqrt{20}$. Results were also obtained for other appropriate choices.
[16] Using integration by parts and periodic boundary conditions, the pattern roughness can be written as $R = \int [(1/D_a) a f(a,h) + (1/D_h) g(a,h)] d\vec{r}$ for stationary patterns.